Mon. Not. R. astr. Soc. (1992) **257**, 476–484

Irradiation of the secondary star in cataclysmic variables

Stephen Davey and Robert Connon Smith
Astronomy Centre, Division of Physics and Astronomy, University of Sussex, Falmer, Brighton BN1 9QH

Accepted 1992 February 12. Received 1992 January 31; in original form 1991 September 9

SUMMARY

This paper shows how the relative strength of the Na I doublet over the surface of the secondary star can be calculated from radial velocity curves obtained using the Na I absorption feature around 8190 Å. The results for 11 dwarf novae and one magnetic cataclysmic binary system are presented. For the five dwarf nova secondary stars that showed significant heating, it is found that the surface distribution is far more asymmetrical than would be expected from irradiation by the white dwarf and disc hotspot. A possible mechanism for this asymmetry is circulation currents induced by the heating of the half of the secondary star's atmosphere facing the disc hotspot. There is also found to be an asymmetrical surface distribution for AM Her which cannot be explained using this argument, since there is no disc in this magnetic system.

Key words: line: formation – stars: atmospheres – binaries: spectroscopic – novae; cataclysmic variables.

1 INTRODUCTION

The Na I doublet around 8190 Å has been detected in many cataclysmic variables (CVs) and the results from the measurements of radial velocities for 12 of them are given here. The details of the observations and data analysis are given in Friend *et al.* (1990a) for U Gem, SS Aur, BD Pav, DO Dra and CN Ori; Friend *et al.* (1990b) for CH UMa, MU Cen, SS Cyg and RU Peg; Martin, Smith & Jones (1989) for IP Peg; Martin (1988) for AM Her; Mateo, Szkody & Garnavich (1991) for YY Dra. It should be noted that YY Dra and DO Dra are believed to be the same object, although they will be referred to by the names used by the different authors in order to help distinguish the two sets of data.

The effects of the heating of the secondary star on its radial velocity curve were seen by Hessman *et al.* (1984) in their observations of SS Cyg during quiescence and outburst. They were also seen by Wade & Horne (1988) in their observations of Z Cha, which showed a decrease in the Na I doublet and TiO absorption strength on the inner face of the secondary star. A simplified model in which the absorption was artificially set to zero in a region around the L_1 point was used to model the TiO and Na I light curves. The size of the zero region was varied until a best fit to the TiO flux data was obtained and the corresponding correction to the measured radial velocity was made. This was then also done using a maximum-entropy model which gives the smoothest possible solution. It was then assumed that the true solution was between the two extremes of the zero-region model and the maximum-entropy model. A more sophisticated computer simulation was performed by Martin *et al.* (1989) to correct their radial velocities for the red star in IP Peg obtained from measurements of the Na I doublet. In that work, a model secondary star was irradiated by the white dwarf and hotspot, and the radial velocities were calculated numerically by assuming that the effect of the irradiation was to ionize some of the sodium atoms on the inner face of the secondary star. Although it was found possible to produce the observed eccentricity of the orbital velocity fit, the model was not able to reproduce the large asymmetry found in the radial velocity curve from the observations. The effect of contamination of the Na I doublet by disc features in that part of the spectrum was also investigated, but did not produce the desired results.

Section 2 presents the radial velocity curves and their use to estimate masses. Section 3 shows the results of reconstructing the surface distribution of the Na I doublet strength from the radial velocity curves. Section 4 discusses the possible mechanisms that could produce the results observed.

2 RADIAL VELOCITY CURVES

2.1 Eccentricities of radial velocity curves

For each object a radial velocity curve was plotted using the data from the observations by Martin (1988), Friend (1988) and Mateo *et al.* (1991). Fig. 1 shows the radial velocity curve for AM Her; the radial velocity curves for all the other objects can be found in the published papers referred to above.

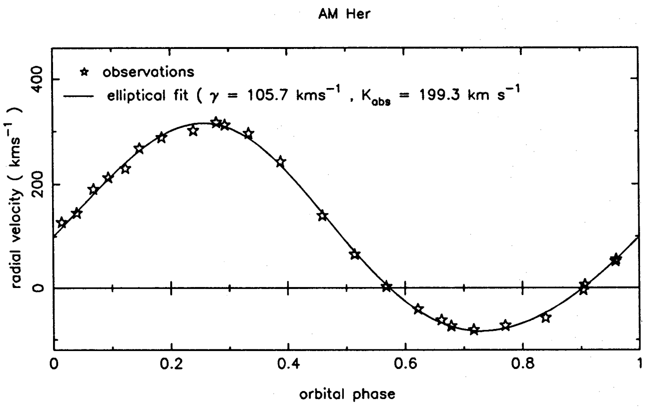

Figure 1. Radial velocity curve for AM Her.

If the orbit were circular, the motion of the centre of mass of the secondary star would be given by

$$V(\phi)=\gamma+K_2\sin(2\pi\phi), \tag{1}$$

where K_2 is the true orbital velocity of the secondary star, γ is the systemic velocity and ϕ is the phase angle of the observation with $\phi=0.0$ at inferior conjunction, i.e. when the red dwarf is in front of the white dwarf. Because cataclysmic binary systems have very short periods, it is generally believed that any initial non-circularity would have been rapidly removed by tidal forces between the red dwarf and the white dwarf, and that the present orbits are indeed circular. However, the radial velocity curve may still be distorted from a pure sine wave by geometrical distortion and heating of the secondary star by its companion, causing the centre of light given by the strength of the Na I doublet to differ from the centre of mass. The effects can be represented by allowing for a phase shift in the sine curve, or more generally by introducing a fictitious eccentricity. The data were therefore fitted with general circular and elliptical orbital fits of the form

$$V_{\rm obs}(\phi)=V_{\rm circ}(\phi)\equiv\gamma+S\sin(2\pi\phi)+C\cos(2\pi\phi) \tag{2}$$

and

$$V_{\rm obs}(\phi)=V_{\rm ell}(\phi)\equiv\gamma+S_1\sin(2\pi\phi)+C_1\cos(2\pi\phi)+S_2\sin(4\pi\phi)+C_2\cos(4\pi\phi). \tag{3}$$

For the elliptical fit the eccentricity is approximated as

$$e=\sqrt{\frac{S_2^2+C_2^2}{S_1^2+C_1^2}}, \tag{4}$$

provided that $e\leq0.1$. Formally, the orbital velocity can be obtained from the semi-amplitudes of these curves, which are

$$K_{\rm abs}({\rm circ})=(S^2+C^2)^{1/2} \tag{5}$$

and

$$K_{\rm abs}({\rm ell})=\left(\frac{S_1^2+C_1^2}{1-e^2}\right)^{1/2}, \tag{6}$$

where the subscript 'abs' indicates that the semi-amplitude is derived from absorption-line measurements and is not the true orbital velocity, K_2, of the secondary star. The relationship between K_2 and $K_{\rm abs}$ will be discussed more fully in the next section.

Table 1. Eccentricities and statistical significance.

Object	Type	Eccentricity	σ_c	σ_e	T_2	Significance
AM Her	AM Her	0.068 ± 0.010	11.78	6.86	19.49	99%
IP Peg	DN	0.100 ± 0.017	30.96	19.93	10.84	99%
U Gem	DN	0.043 ± 0.011	17.67	15.27	6.61	99%
CH UMa	DN	0.090 ± 0.025	8.86	7.49	6.59	99%
YY Dra	DN	0.055 ± 0.018	12.93	10.99	3.46	95%
RU Peg	DN	0.036 ± 0.014	8.18	7.74	2.11	<90%
SS Aur	DN	0.109 ± 0.065	19.33	17.63	1.11	<90%
SS Cyg	DN	0.031 ± 0.015	9.21	8.93	0.92	<90%
BD Pav	DN	0.021 ± 0.012	15.19	14.98	0.52	<90%
DO Dra	DN	0.024 ± 0.015	12.01	11.88	0.29	<90%
MU Cen	DN	0.028 ± 0.020	11.58	11.52	0.14	<90%
CN Ori	DN	0.051 ± 0.051	26.39	27.89	0.00	<90%

Because equations (2) to (6) are the standard representations of circular and elliptical orbits, standard tests can be used to decide whether the elliptical fit is a significantly better fit to the data, and so whether the fictitious eccentricity is statistically significant. The F-test was used (Bassett 1978) with the statistic T_2 calculated as

$$T_2=\frac{1}{2}(N-f)\left(\frac{\sigma_c^2}{\sigma_e^2}-1\right), \tag{7}$$

where N = number of observations, f = number of degrees of freedom for the fit (five in this case), σ_c = rms deviation of the data from the circular fit, σ_e = rms deviation of the data from the elliptical fit.

The 90, 95 and 99 per cent confidence levels are obtained from tables for the F-test with $n_1=2$ and $n_2=N-f$ (Lindley & Scott 1984).

The results from the fits are summarized in Table 1. AM Her, CH UMa, IP Peg and U Gem all show eccentricities significant to the 99 per cent level and YY Dra is just at the 95 per cent confidence level.

In Friend *et al.* (1990b) the eccentricity for SS Aur was found to be 0.17. For the present analysis all the original data were refitted and slightly different eccentricities were found in most cases. For SS Aur the difference was large, with a reduced eccentricity of 0.109. We have no explanation for this large difference, but after careful checking we are confident that the smaller eccentricity is correct. The new eccentricity is not significant and could easily be explained by the poor phase coverage of the observations. Therefore, although the Na I doublet may be contaminated by disc features in the spectrum around 8190 Å, as suggested by Friend *et al.* (1990b), this contamination is not necessary to explain the eccentricity measured for SS Aur.

2.2 Correcting $K_{\rm abs}$ to give the true value of K_2

For those systems that do not show any significant eccentricity, the value of $K_{\rm abs}$ measured from the circular radial velocity curves does not need to be corrected provided that there was not a significantly non-zero phase shift. Indeed, it was found that $C_1\approx0$, within the 1σ errors, for the CVs with insignificant eccentricities and so the value of K_2 is taken to be $K_{\rm abs}$. However, for those objects with a significant eccentricity the value of $K_{\rm abs}$ from the elliptical curves must be corrected, since the irradiation of the front face of the secondary star will move the observed centre of light (as deduced from the Na I absorption lines) away from the L_1 point and give rise to an observed velocity amplitude that is always greater than the true value of K_2. The value of K_2 can be calculated by heating a model star by varying amounts and measuring the eccentricity produced and the corresponding increase in K_2. If the secondary star were not distorted or heated then the radial velocity curve should be fitted by a sine curve given by equation (1). However, the observed amplitude of the $\sin(2\pi\phi)$ term from the elliptical fit is given in equation (3) as S_1. Thus, let

$$\Delta K = S_1 - K_2, \tag{8}$$

so ΔK is the amount by which the measured semi-amplitude has increased due to irradiation of the secondary star by the white dwarf and the accretion disc to give the observed value of S_1. Using the terminology for the 'K-correction' from Wade & Horne (1988) then $\Delta K = fV_{eq}$, where f is the shifting factor and the equatorial velocity of the secondary star is $V_{eq} = \Omega R_{eq}$. For the largest realistic amounts of heating in which the relative strength of the Na I is zero in the front half and 1 in the back half, then $f = 4/3\pi$. For a less extreme case, given, say, by maximum-entropy mapping, the value of f will in general be less than $4/3\pi$. Since V_{eq} is a very weak function of both the mass ratio q and the period, V_{eq} is between 120 and 135 km s^{-1} for all 12 objects, and so $0 \le \Delta K \le 55$ km s^{-1}. Shown in Fig. 2 is a plot of $\Delta K/K_2$ against eccentricity, for various values of q, from a model based on a program by Martin (1988). This method for correcting K_{abs} assumes that the variation in the strength of the Na I doublet over the surface of the secondary star is symmetrical about the L_1 point, which may not be correct, as shown later in Section 3.

Another method for obtaining the true value of K_2 is by fitting a curve only to the radial velocities measured between phases −0.2 and 0.2, when the secondary star is viewed from the back and its appearance should be relatively unaffected by the irradiation from the white dwarf and disc. Because fewer observations are used for the radial velocity fit, which should be circular, the errors in the measured value of K_{abs} are larger. Again it is assumed that the material in the back half of the secondary star is not being heated and that the measured orbital velocity is the true value of K_2. However, if heated material is reaching the back half of the secondary star then the measured K_{abs} will in general be higher than the true K_2.

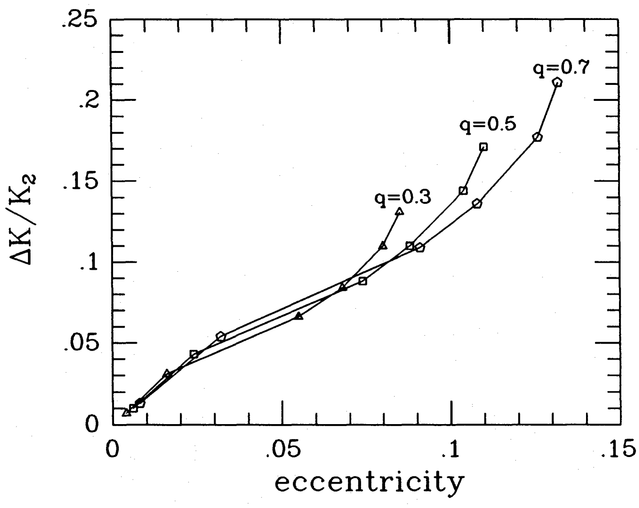

Figure 2. Plot of $\Delta K/K_2$ against eccentricity of the radial velocity curve, using a model for irradiation of the secondary star based on a program by Martin (1988) with increasing amounts of heating. The system parameters used here are those for IP Peg; i.e. period = 3.80 hr, $M_2 = 0.34\ M_\odot$, inclination = 80° and $q = 0.3$, 0.5 and 0.7.

Table 2 gives the values of K_{abs} obtained from the radial velocity curves, the corrected values for K_2 and also the values of K_1 used and the references from which they came. Where the eccentricity measured was not significant, the value of K_2 is the same as K_{abs}. For the objects with significant eccentricity, the value of K_2 comes from fitting a curve to the observations around the back of the star only. The uncertainties quoted for K_{abs} are 1σ errors, whereas the ranges given for K_1 and K_2 are 95 per cent confidence limits calculated from the radial velocity curves which usually fall between 2σ and 3σ errors. We have not attempted here to estimate the systematic errors in K_1 arising from difficulties in interpreting the emission-line observations (e.g. Wade 1985, section 4.5). The ranges for the mass ratios are calculated from $q = K_1/K_2 = M_2/M_1$ unless K_1 was not available from the literature, in which case q was calculated from the main sequence (MS) assumption (see below) or from rotational broadening (Friend *et al.* 1990a, b).

2.3 Mass determinations from main-sequence assumptions

From the values of K_1 and K_2 the range of $q = M_2/M_1$ can be calculated, and when combined with a suitable M_2–period relation, the mass range for the white dwarf, M_1, is obtained. These results are summarized in Table 3, which also gives

Table 2. Measurements from observations.

Object	$q = M_2/M_1$	K_{abs}(kms^{-1})	K_2(kms^{-1})	K_1(kms^{-1})	Spectral Type
AM Her	0.22 - 0.37†	199.3 ± 2.0	175 - 199	?	M2 - M6
IP Peg	0.42 - 0.75	331.7 ± 5.3	280 - 332	140 - 210[b]	M1 - M6
U Gem	0.38 - 0.58	307.0 ± 3.3	275 - 307	117 - 157[c]	M4 - M7
CH UMa	0.34 - 0.78	77.2 ± 2.1	64 - 77	26 - 50[a]	K7 - M0
YY Dra	0.42 - 0.85	190.8 ± 3.7	160 - 203	86 - 136[d]	M3 - M4
RU Peg	0.68 - 0.88	121.1 ± 1.9	116 - 126	86 - 102[c]	K3
SS Aur	0.25 - 0.62	166.3 ± 5.6	152 - 182	45 - 95[f]	M1
SS Cyg	0.54 - 0.66	154.7 ± 2.4	146 - 162	87 - 97[g]	K5
BD Pav	0.35 - 0.56*	278.1 ± 3.2	270 - 286	?	K7
DO Dra	0.40 - 0.70	202.2 ± 3.1	194 - 210	85 - 135[d]	M3 - M5
MU Cen	0.43 - 0.91*	167.2 ± 2.9	160 - 176	?	M1
CN Ori	0.53 - 0.91	218.5 ± 9.6	195 - 239	127 - 177[e]	M4

References: [a]Thorstensen (1986); [b]Marsh (1988); [c]Stover (1981); [d]Williams (1983); [e]Mantel *et al.* (1987); [f]Shafter & Harkness (1986); [g]Hessman *et al.* (1984). †From MS assumption (Martin 1988). ⋆ q from rotational broadening (Friend *et al.* 1990a, b).

Table 3. Results from main-sequence assumption using the relation for M_2 given by equation (11).

Object	P(hours)	$M_2/M_\odot$	$M_1/M_\odot$	Inclination	Spectral Type
AM Her	3.09	0.26	0.55 - 1.04	30° - 33°	M3
IP Peg	3.80	0.34	0.45 - 0.81	$\sin i > 1$	M4
U Gem	4.25	0.38	0.66 - 1.00	$i > 72.4°$	M3
CH UMa	8.23	0.83	1.06 - 2.44	12° - 19°	G8
YY Dra	3.96	0.35	0.41 - 1.12	39° - 65°	M3
RU Peg	8.99	0.95	1.08 - 1.40	32° - 37°	G4
SS Aur	4.39	0.40	0.65 - 1.60	26° - 45°	M2
SS Cyg	6.60	0.65	0.98 - 1.20	36° - 41°	K4
BD Pav	4.30	0.39	0.70 - 1.11	$i > 60.6°$	M2
DO Dra	3.97	0.36	0.51 - 0.90	43° - 66°	M3
MU Cen	8.21	0.86	0.95 - 2.00	34° - 58°	G7
CN Ori	3.95	0.36	0.40 - 0.68	$i > 58.9°$	M3

the predicted spectral type and allowable inclination range from the main-sequence assumption.

The relations used here to obtain the main-sequence mass for the secondary star are Echevarría's (1983) mass–radius relation from the data by Popper (1980) for visual and spectroscopic binary systems

$$\left(\frac{R}{R_\odot}\right)=\alpha\left(\frac{M}{M_\odot}\right)^\beta, \qquad \alpha=1.057, \qquad \beta=0.906, \tag{9}$$

and Eggleton's (1983) formula for the Roche lobe radius R_L in terms of the binary separation a,

$$\left(\frac{R_L}{a}\right)=\frac{0.49q^{2/3}}{0.6q^{2/3}+\ln(1+q^{1/3})}=f(q). \tag{10}$$

This gives a mass–period–q relation:

$$\left(\frac{M_2}{M_\odot}\right)=\left[\frac{GM_\odot}{R_\odot^3}\left(\frac{P(\mathrm{s})}{2\pi}\right)^2\frac{f^3(q)}{\alpha^3}\left(\frac{1+q}{q}\right)\right]^{1/(3\beta-1)}, \tag{11}$$

in which the dependence on q is very weak. The spectral types are calculated using Echevarría's (1983) mass and spectral type relation.

Patterson's (1984) mass–period relation,

$$\left(\frac{M_2}{M_\odot}\right)=\begin{cases}0.071P^{1.21}(\mathrm{hr}) & 0.4\le M_2/M_\odot\le 0.8,\\ 0.116P(\mathrm{hr}) & 0.8\le M_2/M_\odot\le 1.4,\end{cases} \tag{12}$$

which was used by Friend *et al.* (1990a,b), gives slightly larger values (by about 10 per cent) for M_2 compared to those given in Table 3. The corresponding values for M_1 would increase and the predicted spectral types would need to be suitably altered. For IP Peg it is found that $\sin i>1$ for all values of q in the allowable range, and so there is no value of q that agrees with the inclination $79.3° \pm 0.9°$ obtained from eclipse data (Marsh 1988). Hence, either the main-sequence assumptions cannot hold in this case or, perhaps more likely, the value of K_1 is not correct. This is also true for U Gem, for which the measured inclination is $69.7°\pm0.7°$ (Zhang & Robinson 1987) and is below the limiting value of $i>72.4°$ from the main-sequence assumption (assuming 95 per cent confidence limits on K_1 and K_2). For BD Pav and CN Ori, the only other eclipsing systems here, the inclinations are measured at about 75° (Friend *et al.* 1990a) and 67° ± 3° (Mantel *et al.* 1987) respectively, which are within the allowable range for the main-sequence assumption. It is also found for CH UMa, MU Cen, RU Peg and SS Aur that some of the possible values for M_1 are greater than the 1.4-$M_\odot$ limiting mass, but since the range of values is so large this constraint on the main-sequence assumption cannot be used until the ranges for q are better known and/or K_1 is more reliably determined.

3 SURFACE MAPPING OF THE SECONDARY STAR

For the five objects, AM Her, CH UMa, IP Peg, U Gem and YY Dra, that all show significant eccentricities, the heating of the surface can be calculated. Having estimated the true value of K_2 the sine curve given by equation (1), which is from the orbital motion of the secondary star, can be subtracted from the observed radial velocities. The purpose of this subtraction is to remove the large dynamical contribution to the radial velocity curve and reveal the much smaller contribution due to irradiation (*cf.* Figs 1 and 3). The uncertainty in the estimate of K_2 gives rise to a corresponding uncertainty in the effect of irradiation, but the results are not very sensitive to the exact value of K_2. The residual velocities produced would then be fitted by the curve

$$v(\phi)=\Delta K\sin(2\pi\phi)+C_1\cos(2\pi\phi)+S_2\sin(4\pi\phi)+C_2\cos(4\pi\phi), \tag{13}$$

where ΔK is given in equation (8) and C_1, S_2 and C_2 are given in equation (3). The calculated residual velocities are plotted in Figs 3–7, although the residual velocity fits have not been shown.

It is assumed that the residual velocities found are solely due to the distorted Roche lobe shape and the uneven heating of the secondary star, and that contamination from disc emission features around the 8190-Å region are not important. The coordinate system used is with the x-axis along the line of centres, the y-axis in the plane of the orbit, and the z-axis parallel to the rotation axis of the system, forming a right-handed set with its origin at the centre of the secondary star.

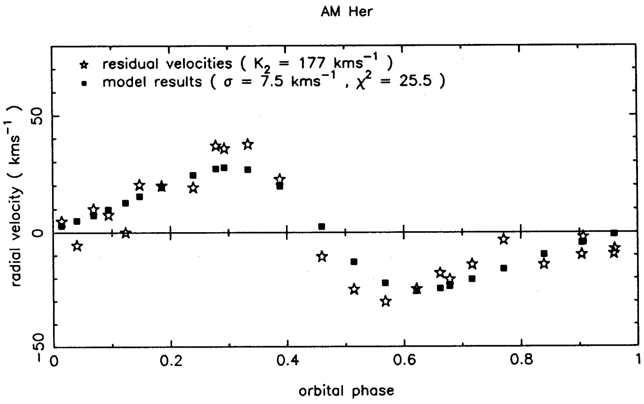

Figure 3. Residual velocity curve for AM Her (open stars) and synthetic velocity curve (filled squares).

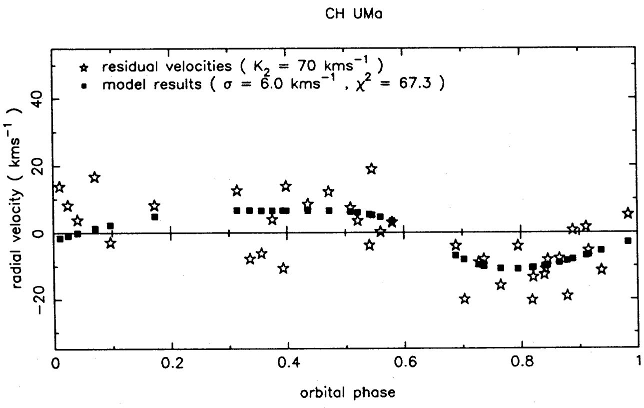

Figure 4. Residual velocity curve for CH UMa.

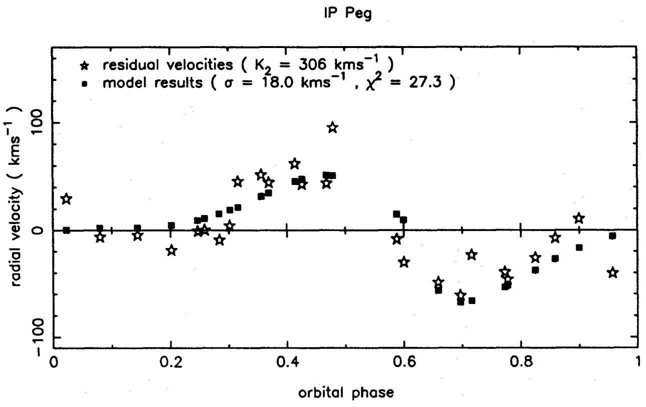

Figure 5. Residual velocity curve for IP Peg.

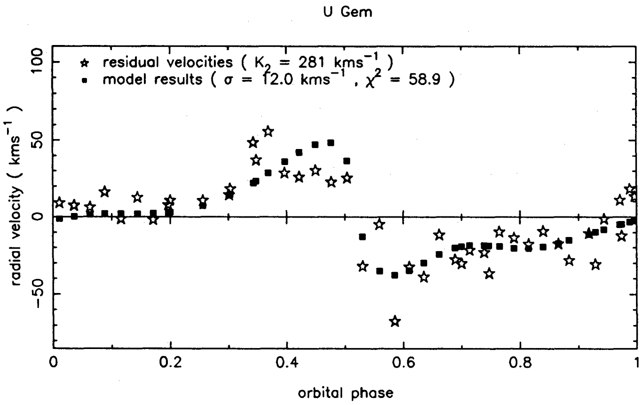

Figure 6. Residual velocity curve for U Gem.

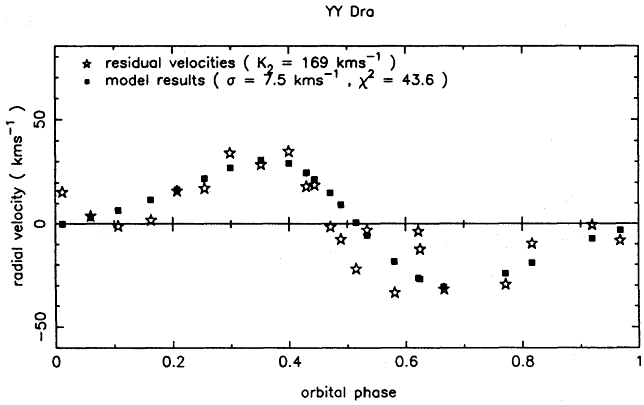

Figure 7. Residual velocity curve for YY Dra.

The relative strength of the Na I doublet over the surface of the secondary star is parametrized by the equation

$$I(\theta,\ \zeta)=1.0+\sin\theta\sum_{n=1}^{3}\left[a_n\cos(n\zeta)+b_n\sin(n\zeta)\right],\qquad(14)$$

where θ and ζ are the standard spherical polar and azimuthal angles. θ is measured from the positive z-axis and ζ is measured anticlockwise from the positive x-axis in the xy-plane. When $I(\theta,\ \zeta)$ is less than zero it is set to zero and, similarly, when $I(\theta,\ \zeta)$ is greater than 1 it is set to 1, and so $0.0 \leq I(\theta,\ \zeta) \leq 1.0$. The surface of the secondary star is divided up into small elements with the strength of the Na I doublet for each element given by equation (14). Shielding by the disc at the L_1 point and around the equator of the secondary star is included by setting $I(\theta,\ \zeta)=1$ in a band extending about 5° above and below the equator, where there would be no direct irradiation from the white dwarf. Limb darkening has also been included although the effect of gravity darkening has been assumed to be small and is not included in this model; see Martin (1988) for details. The values of the coefficients a_n and b_n are initially guessed and a synthetic residual radial velocity curve, $V_{\rm syn}(\phi)$, is obtained for the intensity distribution $I(\theta,\ \zeta)$ using a simulation program by J. S. Martin (Martin *et al.* 1989) that mimics the method used to measure the radial velocities from the observations. The same orbital phases as the original observations are used and the goodness-of-fit between the synthetic residual velocities and the observed residual velocities is calculated using the χ^2 statistic,

$$\chi^2=\sum_{k=1}^{N}\left[\frac{V_{\rm res}(k)-V_{\rm syn}(k)}{\sigma(k)}\right]^2.\qquad(15)$$

Here, $\sigma(k)$ is the rms deviation for each observation k at orbital phase $\phi(k)$. Since these are not known in general the values of $\sigma(k)$ are taken to be the same, usually σ_e, for all phases. The coefficients a_n and b_n are suitably corrected until the smallest value of χ^2, i.e. the best fit, is reached and the convergence stops. The resulting synthetic radial velocity curves are shown in Figs 3–7 and the corresponding maps of the surface distribution of the Na I doublet are shown in Figs 8–12. The surface maps obtained are relatively unaffected by choosing K_2 in the range allowable to be consistent with the observed eccentricities. In particular, the phase angle of the terminator does not appear to change significantly as K_2 is varied. The view of the secondary star is from the top looking down the z-axis with the white dwarf to the right along the x-axis. The units on the axes are arbitrary but are the same for each object. The small-scale details are probably artefacts of the truncated series used to calculate $I(\theta,\ \zeta)$ and also the

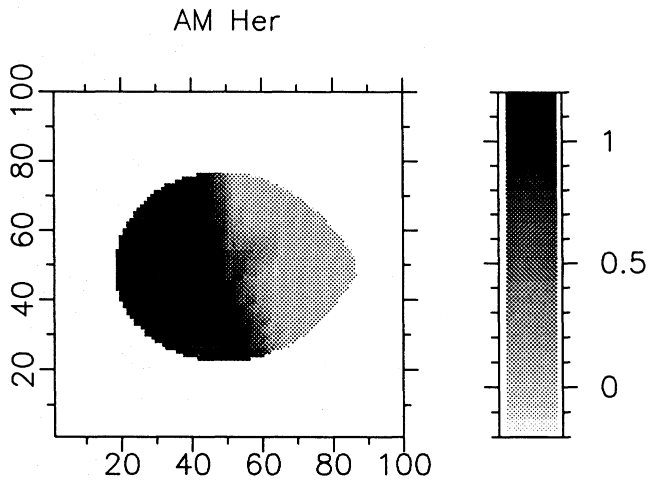

Figure 8. Surface map of AM Her showing the relative strength of the Na I doublet.

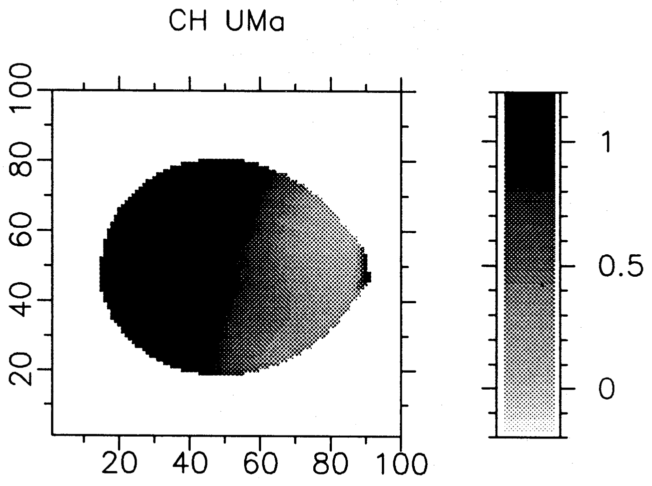

Figure 9. Surface map of CH UMa.

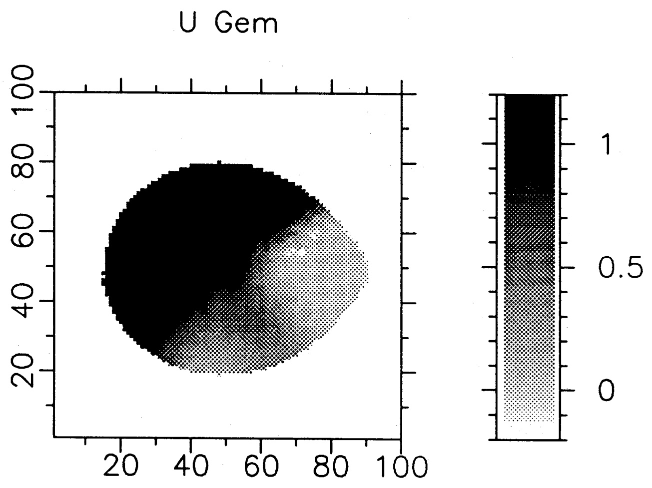

Figure 11. Surface map of U Gem.

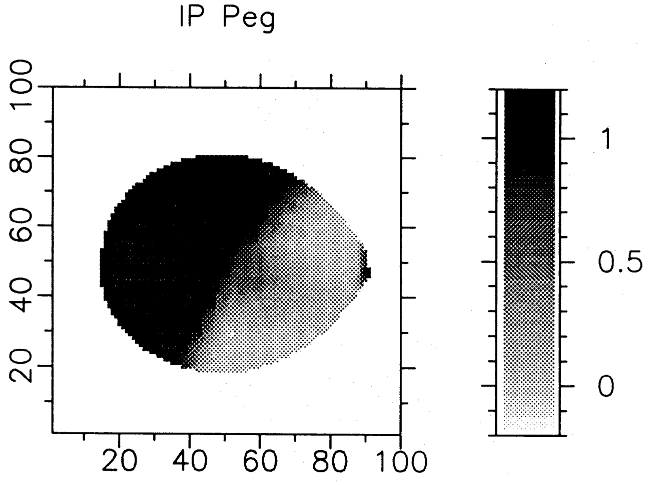

Figure 10. Surface map of IP Peg.

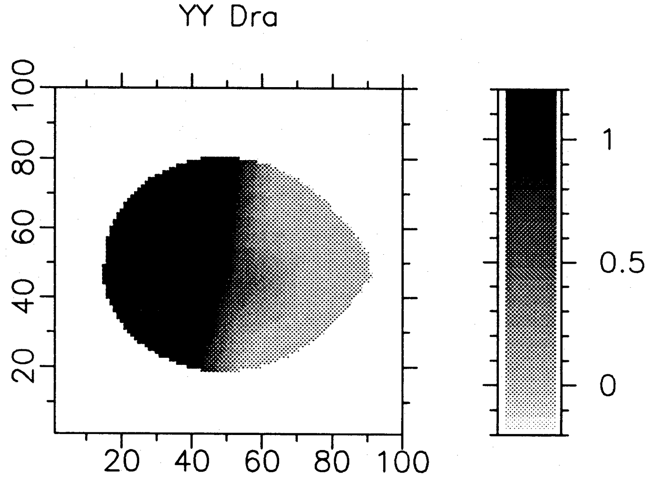

Figure 12. Surface map of YY Dra.

coarseness of the surface grid, but the overall asymmetry of the distribution is genuine. This was tested by performing the simulation with a spherical polar coordinate system along the x-axis, so that the L_1 point was at the pole, and the results were qualitatively the same. Since the strength of the Na I doublet is related to the temperature at the surface (Brett & Smith, in preparation), these plots also give an indication of the temperature distribution over the secondary star.

Ideally, we would use the observed variation of the Na I line strength around the orbit to put further constraints on the intensity distribution model. Unfortunately, the observations we have used did not include spectrophotometric measurements, so we do not have reliable information on the variation of the flux deficit. However, we have plotted in Fig. 13 the estimated flux deficits for IP Peg and U Gem, derived from the original spectra using

$$fd(\text{Na I}) = \int_{8170}^{8220} [c(\lambda) - f(\lambda)]\, d\lambda, \qquad (16)$$

where $c(\lambda)$ is the mean continuum level and $f(\lambda)$ is the profile of the Na I doublet (Wade & Horne 1988). The model curves in Fig. 13 were calculated from synthetic spectra generated by J. S. Martin's program, using the same definition for the flux deficit. The inputs for the synthetic spectra were the best-fitting intensity distribution maps (Figs 10 and 11). Although there is a large scatter in the observed flux deficits, because no photometric calibration was available, the predicted curves are not inconsistent with the observed points. This gives us some additional confidence in our results.

4 DISCUSSION

4.1 Results from surface mapping

The most striking result from the Na I doublet distribution maps for the dwarf novae with significant eccentricities is that the secondary star seems to be strongly irradiated from a direction that is not centred on the L_1 point, but instead towards the leading side of the star (along the negative y-axis). This is most obvious for IP Peg and U Gem, shown in Figs 10 and 11, which appear to be heated some distance into the back half of the star as though they were illuminated from a direction about 45° away from the line of centres.

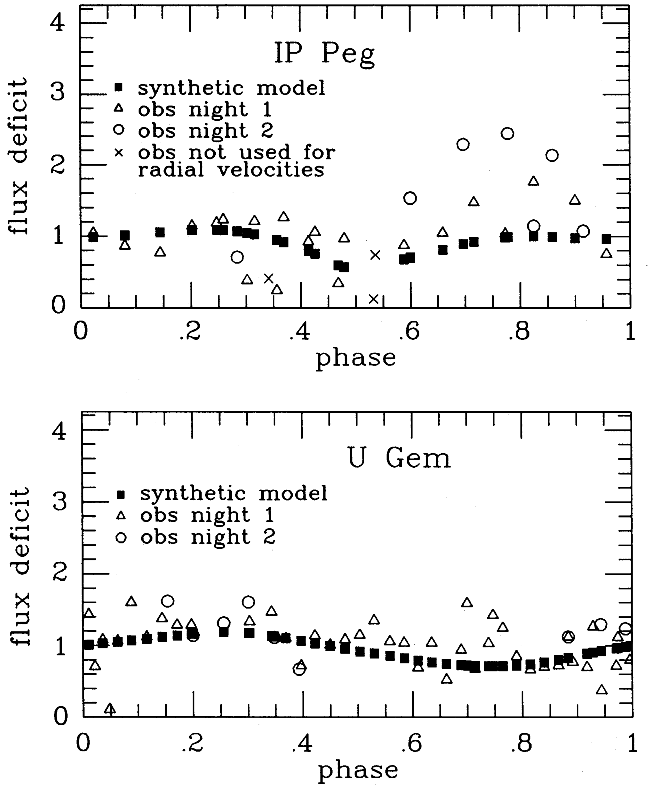

Figure 13. These figures show the observed flux deficits for IP Peg and U Gem and the corresponding model results for the observed phases. The results have been normalized by the mean of the flux deficits between orbital phases −0.15 and 0.15.

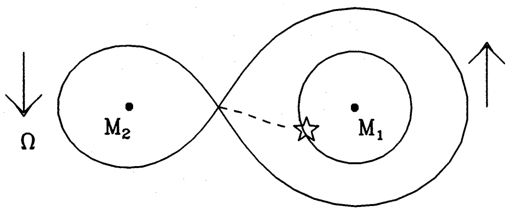

Figure 14. Sketch of a typical dwarf nova with disc and hotspot.

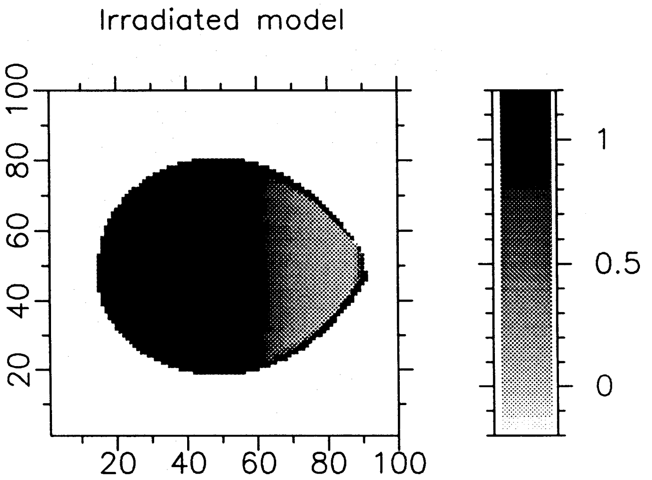

Figure 15. Surface map from an irradiated secondary star model with equal heating from the white dwarf and the hotspot.

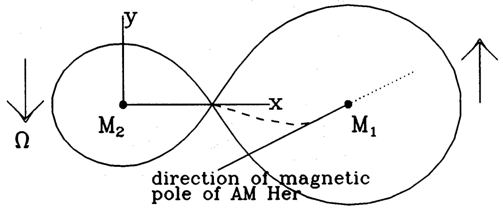

Figure 16. Sketch of the magnetic CV AM Her showing direction of accretion pole.

Although the hotspot on the disc surrounding the white dwarf is on the same side as the hot area on the secondary star, the angle between the line of centres and the line joining the secondary star and the disc hotspot is only about 15° – see Fig. 14. As mentioned earlier from the work by Martin (1988), the position of the white dwarf and hotspot on its disc would give rise to irradiation that was not far from being symmetrical about the L_1 point. This is shown in Fig. 15 which is a computed model for a secondary star heated equally by the white dwarf and the disc hotspot.

Since the distribution maps cannot be explained by direct irradiation, an additional mechanism is necessary, such as motions induced by heating of the surface layers of the secondary star. Numerical work by Kırbıyık (1982), which considered circulation currents in a spherical radiative star, found that currents driven by strong heating could penetrate 16° into the dark side of the star in both directions. In the case of a CV the red dwarf is of around 0.5 $M_\odot$ and so would be expected to be fully convective, destroying any possible large-scale circulation of material. However, it is possible that the combined heating by the white dwarf and disc hotspot is sufficient to suppress the convection in the outer atmosphere of the secondary star due to the reduced temperature gradient (Brett & Smith, in preparation). If the secondary star has a radiative atmosphere in this region then circulation currents could start from the hotter L_1 point towards the cooler half of the star. On the other side of the L_1 point there is no heating from the disc hotspot to suppress the convection and so material would not circulate easily. This would lead to a Na I doublet distribution that is asymmetric about the L_1 point, and hence the asymmetry observed in the radial velocity curves.

This explanation cannot apply, though, for the results shown in Fig. 8 for AM Her which is a magnetic CV and so has no disc. Here the irradiation is by the white dwarf and accretion column only, and would be expected to be fairly symmetrical about the L_1 point instead of being stronger on the trailing side, compared to the results for the dwarf novae. It is also believed that the magnetic pole of AM Her (Cropper 1988) points towards the leading side of the secondary star, as shown in Fig. 16. Since this was the only magnetic star for which data were available for mapping the surface distribution, an explanation or confirmation of this result is difficult to find.

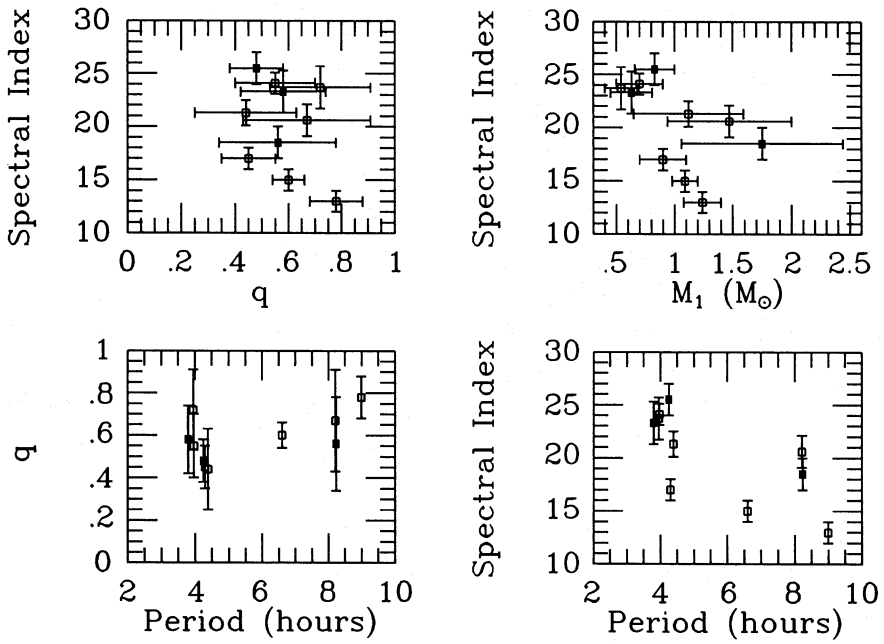

Figure 17. Plots of pairs of parameters for the dwarf novae. Filled squares are heated secondary stars and open squares represent unheated secondaries.

4.2 Contradictory results for DO Dra and YY Dra

There is still the problem of explaining why DO Dra and YY Dra give different results even though they are supposed to be the same object. The observations were obtained in 1987 March and June respectively, and yet by 1987 June the secondary star had acquired a significant eccentricity to its radial velocity curve and hence was showing signs of strong heating. One possible explanation, that there had been an outburst much closer to one set of the observations than to the other, is unlikely as no outbursts were seen in this system around these dates (G. M. Hurst, private communication). Another possible explanation is that the 95 per cent significance of the eccentricity of YY Dra's radial velocity curve is not significant enough and just occurred by chance. If this was the case then the values of K_2 obtained would be 181–203 km s^{-1} for YY Dra and 194–210 km s^{-1} for DO Dra, which do overlap at the 95 per cent confidence level. Another possibility is that they are not the same system but just happen to have very similar orbital parameters!

Of the 11 dwarf novae studied, there does not appear to be any obvious difference between those that show significant heating and those that do not.* The possible parameters measurable from observations that can vary between systems are period, mass ratio (q) and spectral type, and M_1 (a function of q and period) from the main-sequence assumption. The spectral index is defined here as G0 = 0, K0 = 10, M0 = 20, etc. There does not appear to be any single parameter or a combination of pairs of parameters that determines whether a secondary star is strongly heated or not. Fig. 17 shows plots of different pairs of parameters, with the filled squares being the heated dwarf nova secondary stars and the open squares the unheated secondary stars. The uncertain results for YY Dra are not plotted as they would overlap those for DO Dra. The only other possible difference is that CH UMa, IP Peg and U Gem appear to be much further from the MS assumption than the others, although this is probably not surprising since they are the ones being heated most strongly.

*Indeed, if DO Dra and YY Dra are truly showing different results, then it is possible for the same object to show signs of heating at one time but not another, and hence there need not be any difference between those that are heated and those that are not.

5 CONCLUSIONS

The mapping over the surface of the strength of the Na I doublet from residual velocity curves has shown that, for some secondary stars, the correction to obtain the true value of K_2 can be around 30 km s^{-1} due to the effects of irradiation. There is also evidence that the heating is more asymmetric than would be expected from a direct irradiation model. For the dwarf novae CH UMa, IP Peg, U Gem and YY Dra, we speculate that asymmetric heating may have led to circulation currents on the leading side of the secondary star only. This possibility, that one-sided circulation currents are occurring, needs further investigation by suitable numerical work, modelling the surface of a convective star by solving the hydrodynamic equations or by using a suitably modified Smoothed Particle Hydrodynamics N-body code. An explanation of the results for AM Her is also necessary, either from further observations of magnetic CVs to confirm these results, or from a better understanding of the effects of the white dwarf's strong magnetic field on the atmosphere of the secondary star. Further observations of dwarf novae are also necessary to help explain why some show signs of being heated much more strongly than others, and to explain the contradictory results for DO Dra and YY Dra. The mapping of the secondary star's atmosphere could also be made more sophisticated by using a maximum entropy type program rather than the fairly crude truncated Fourier series used for $I(\theta, \zeta)$ here. The surface would then be defined by the relative strength of the Na I doublet over a patchwork of surface elements.

ACKNOWLEDGMENTS

We would like to thank Dr A. C. Cameron for many helpful comments on this paper and for much useful discussion. We are also very grateful to J. S. Martin for the use of her radial velocity simulation program. We also thank the anonymous referee for many helpful comments. This paper and the results contained herein were all produced using the STARLINK node at the University of Sussex. SCD is in receipt of an SERC research studentship.

REFERENCES

Bassett, E. E., 1978. *Observatory,* **98,** 122.
Cropper, M., 1988. *Mon. Not. R. astr. Soc.,* **231,** 597.
Echevarría, J., 1983. *DPhil thesis,* University of Sussex.
Eggleton, P. P., 1983. *Astrophys. J.,* **268,** 368.
Friend, M. T., 1988. *DPhil thesis,* University of Sussex.
Friend, M. T., Martin, J. S., Smith, R. C. & Jones, D. H. P., 1990a. *Mon. Not. R. astr. Soc.,* **246,** 637.
Friend, M. T., Martin, J. S., Smith, R. C. & Jones, D. H. P., 1990b. *Mon. Not. R. astr. Soc.,* **246,** 654.
Hessman, F. V., Robinson, E. L., Nather, R. E. & Zhang, E.-H., 1984. *Astrophys. J.,* **286,** 747.
Kırbıyık, H., 1982. *Mon. Not. R. astr. Soc.,* **200,** 907.
Lindley, D. V. & Scott, W. F., 1984. *New Cambridge Elementary Statistical Tables,* Cambridge University Press, Cambridge.
Mantel, K. H., Barwig, H., Haefner, R. & Schoembs, R., 1987. *Cataclysmic Variables, Recent Multi-Frequency Observations and Theoretical Developments, IAU Colloq. No. 93,* p. 501, eds Dreschel, H., Kondo, Y. & Rahe, J., Reidel, Dordrecht.
Marsh, T. R., 1988. *Mon. Not. R. astr. Soc.,* **231,** 1117.
Martin, J. S., 1988. *DPhil thesis,* University of Sussex.
Martin, J. S., Smith, R. C. & Jones, D. H. P., 1989. *Mon. Not. R. astr. Soc.,* **240,** 519.
Mateo, M., Szkody, P. & Garnavich, P., 1991. *Astrophys. J.,* **370,** 370.
Patterson, J., 1984. *Astrophys. J. Suppl.,* **54,** 443.
Popper, D., 1980. *Ann. Rev. Astr. Astrophys.,* **18,** 115.
Shafter, A. W. & Harkness, R. P., 1986. *Astr. J.,* **92,** 658.
Stover, R. J., 1981. *Astrophys. J.,* **248,** 684.
Thorstensen, J. R., 1986. *Astr. J.,* **91,** 940.
Wade, R. A., 1985. In: *Interacting Binaries, NATO Advanced Study Institute,* p. 289, eds Eggleton, P. P. & Pringle, J. E., Reidel, Dordrecht.
Wade, R. A. & Horne, K., 1988. *Astrophys. J.,* **324,** 411.
Williams, G., 1983. *Astrophys. J. Suppl.,* **53,** 523.
Zhang, E.-H. & Robinson, E. L., 1987. *Astrophys. J.,* **321,** 813.